Supplementary Information

Supplementary Material and Methods

Zebrafish transgenic lines

We used the following fish lines: WT AB strain, *ET(krt4:EGFP)*$^{sqet33\text{-}mi60A}$ (*ET33-mi60A*), *ET(krt4:EGFP)*$^{sqet33\text{-}1A}$ (*ET33-1A*) (Poon et al., 2010), *Tg(hsp70l:Gal4)*^{kca4}*;Tg(UAS:myc-Notch1a-intra)*^{kca3}, [abbreviated here as *Tg(UAS:NICD)*] (Scheer et al., 2001), and *Tg(fli1a:GFP)y1* (Lawson and Weinstein, 2002), *Tg(myl7:mRFP*) (Rohr et al., 2008).

Treatments

Heat shocks to *Tg(UAS:NICD)* fish were applied automatically as described (Munch et al., 2013). Regimes for heat shock applications of each experiments are indicated in the corresponding figure. For short-term experiments (1-3 dpci, 1-7 dpci) we applied 40 min heat shocks and for long-term experiments (1-33 dpci, 1-90 dpci) a 1-h heat shock. Control animals for these experiments were *Tg(hsp70l:Gal4)*^{kca4} or *Tg(UAS:myc-Notch1a-intra)*^{kca3} fish. BrdU (30 µl, 2.5 mg/ml in PBS) was administered intraperitoneally at 2 dpci (for endocardial proliferation analysis) or at 5 and 6 dpci (for myocardial proliferation analysis).

Histology

All antibodies used in our studies have been tested elsewhere. We used the following antibodies: GFP (1:100, Living Colors, rabbit, C#632592, and mouse, C#632381) (Gonzalez-Rosa et al., 2011), GFP (1:500, Aves, chicken, GFP-1010) (Zhang et al., 2013), BrdU (1:30, BD, ab6326) (Munch et al., 2013), Delta-4 (1:100, Santa Cruz Biotechnology, rabbit, sc-28915) (D'Amato et al., 2016), collagen type I (1: 100, DSHB, SP1.D8, mouse, C#SP1.D8,RRID:AB_528438) (Gonzalez-Rosa et al., 2011), myosin heavy chain (1:100,

MF20, DSHB, mouse, C#MF20RRID:AB_2147781) (Gonzalez-Rosa et al., 2011), ERG (1:200, Abcam, rabbit, ab110639) (Bednarek et al., 2015) and Mef-2 (1:100, Santa Cruz Biotechnology, rabbit, sc-313) (Bednarek et al., 2015) Phalloidin Congutated to FITC (1:50, Sigma-Aldrich, P5282). For IHC against Delta-4 and collagen type-1 the signal was amplified with secondary antibodies coupled to horseradish peroxidase (1:100, Dako Cytomation, P0447-8) and tyramides coupled to Cy3 (1:100, TSA, Perkin Elmer, NEL744001KT) (Luxan et al., 2013). ISH was performed as described (Kanzler et al., 1998) using the following probes: *atf3* (Chen et al., 2012), *lfng* (Prince et al., 2001), *hand2* (Yelon et al., 2000), *nkx2.5* (Chen and Fishman, 1996), *notch1b*, *notch2*, *notch3* (Westin and Lardelli, 1997), *cdh5* (Larson et al., 2004), *mmp9*, *nfatc1a, klf2a* (Vermot et al., 2009) and *l-plastin* (Yoshinari et al., 2009). Primer sequences for new probes can be found in Table S7. For fluorescence ISH (FISH), we followed the same protocol (Kanzler et al., 1998), however we used a peroxidase-coupled antibody for DIG-labelled mRNA-probe detection. We developed the signal using tyramides coupled to Cy3 (TSA, Perkin Elmer, 1:200) and subsequently performed IHC after several washed with PBS. AFOG staining was as described previously (Kikuchi et al., 2011).

Imaging

Whole mount images were obtained with an Olympus DP71 camera fitted to a Leica stereomicroscope. For whole mount 3D imaging, hearts were fixed in 2% PFA overnight. Following 3 washes in PBS, hearts were incubated in CUBIC reagent 1 (Susaki et al., 2014) at 37ºC overnight. Using a Leica TCS SP-5 confocal microscope, we scanned 900 µm of whole hearts (Figs. 1G-J, 4D, S1E) taking z-stacks every 7 µm with a 10x objective or 200 µm with z-stacks every 3 µm for imaging with the 20x objective (Figs. 2A,2C,3C,4F,S5E). Images of ISH and immune-stained heart sections were taken with a DP71 camera fitted to an Olympus BX51 microscope. For confocal images of immune-stained heart sections, we used a Leica TCS SP-5 or Nikon A1-R confocal microscope.

Gene expression analysis

Power SYBR Green Master Mix (Applied Biosystems) was used for qPCR with the ABI PRISM 7900HT FAST Real-Time PCR System. Gene expression levels were calculated relative to *elf1a* or *rpsm* and then compared with gene activation in samples taken from non-injured hearts (wild-type gene expression analysis) from DMSO-treated samples (for RO treatment experiments) or from *Tg(hsp70l:Gal4)*^{kca4} or *Tg(UAS:myc-Notch1a-intra)*^{kca3} heart samples (for Notch overactivation experiments). RNA-extraction

and cDNA synthesis of PAVEC were conducted accordingly. Quantitative RT-PCR was performed as described before. Data shown represent the mean ± s.d. of three separate experiments. Gene expression levels were calculated relative to *GADPH* and then compared with gene activation DMSO-treated samples.

Quantification and statistical analysis

Experiments were performed on 3- 9 biological replicates to ensure adequate statistical power to detect specific effects. Detailed information on the sample size of each experiment can be found in Table S1 and Table S2.

For 3D volume rendering and volume quantification, we used IMARIS x64 software, with manual selection of the injured region (myl7:mRFP). A mask of this region was used to select the GFP^+ endocardium within the injury site, and the volumes of both were calculated and compared (See Fig. 1K). Graphs represent values of individual hearts and means ± standard deviation (s.d.). Statistical significance was calculated with One-way ANOVA combined with the Newman-Keuls method for multiple comparisons. Filopodia like protrusions of the injury-induced endocardium (Figs. 2C, D, 3H,I) were quantified on randomly selected regions (513 µm x 513 µm x 10 µm) within the whole scanned region, 3-5 per heart. The graphs represent mean values of individual hearts and means ± s.d. Statistical significance was calculated with Student's t-test.

The amount of fibrotic tissue on AFOG-stained heart sections, labelling fibrin and collagen deposition, was measured as follows. ImageJ/ Fiji (http://imagej.net/ImageJ) was used to determine the size of the injured area relative to the size of the ventricle on at least four sections taken at four different levels throughout the heart, so that the size of the injury site at different levels of the heart was represented. The mean value was then calculated. This allows estimation of the 3D volume of the injury site. For quantifications of immunofluorescent or ISH stainings, heart sections were selected randomly. It was assured that the injury site throughout the heart was represented by staining one slide containing sections of different levels of the heart (see Histology section). BrdU incorporation was estimated as the ratio of BrdU-labelled $Mef2^+$ cardiomyocytes to the total number of $Mef2^+$ cardiomyocytes flanking the injured area. We analysed 7-8 hearts and 4-8 sections per heart. Accordingly, endocardial cell proliferation and the percentage of endocardial cells expressing *serpine1* were estimated using 4- 6 hearts per time point and condition and analysing 4- 6 sections per heart. For macrophage quantification, only *l-plastin*- or

mpeg1-expressing cells within the injury site but not in the outer epicardial region were considered. To estimate cardiomyocyte density, the number of $Mef2^{+}$ cardiomyocytes adjacent to the injury site was divided by their area. Graphs represent values of individual hearts and means ± standard deviation. We expected normal distributions of the parameters analysed in our experiments, with similar variances in the experimental groups. Statistical significance was calculated with the two-tailed Student's t-test or with One-way ANOVA combined with the Newman-Keuls method for multiple comparisons.

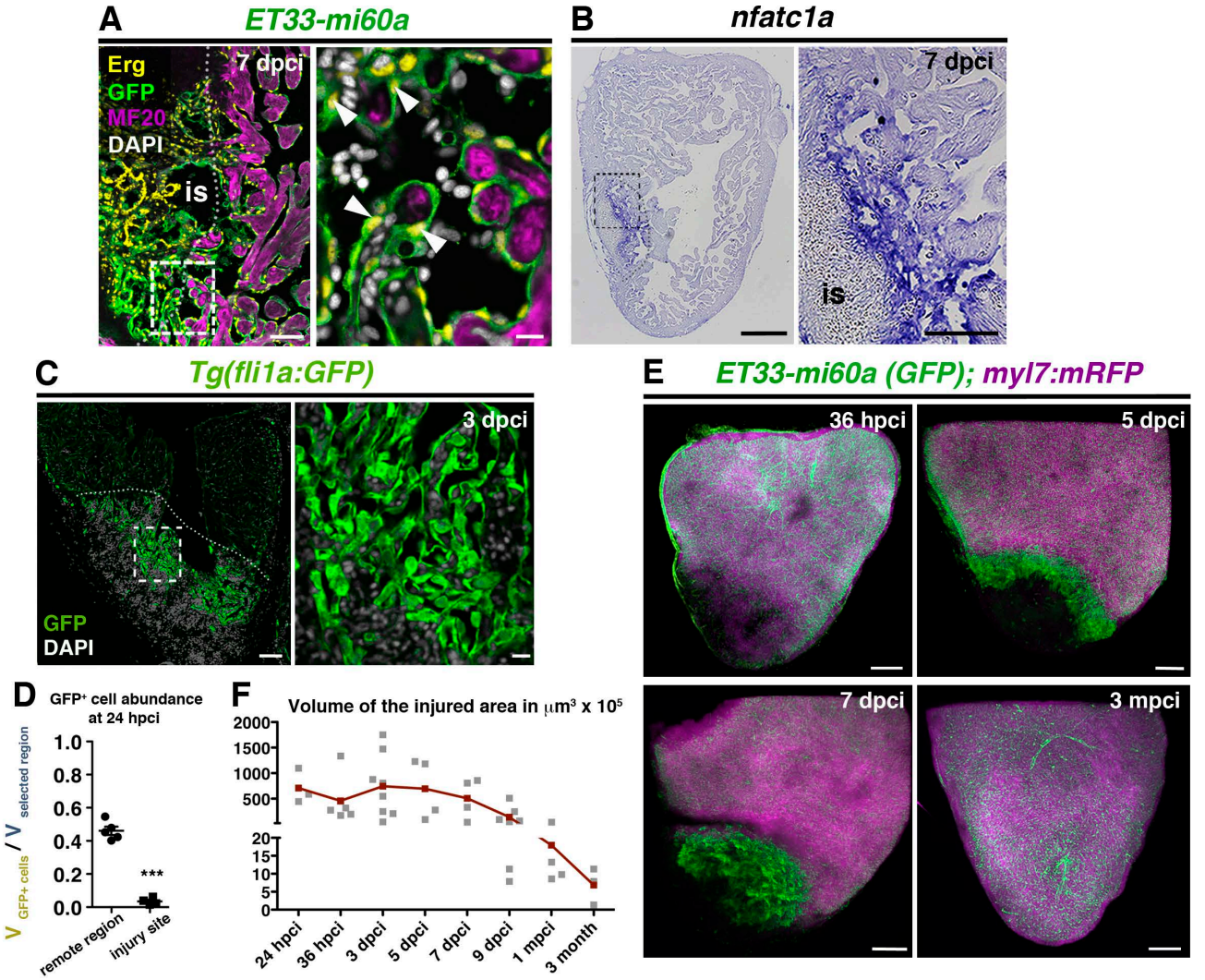

Fig. S1: Activated endocardium in the injury site

(A) IHC against ERG, GFP and MF20 on sections of *ET33-mi60a* transgenic hearts (7 dpci), showing GFP^+ endocardial/endothelial cells within and lining the injury site (is) (white arrowheads). The boxed area is magnified in the right-hand panel. (B) ISH against *nfatc1a* at 7 dpci, showing strong expression within the injury site (is). (C) IHC against GFP on sections of *Tg(fli1a:GFP)* transgenic hearts (3 dpci) showing endocardial cells at the injury site. The boxed area is magnified in the right-hand panel. (D) Scatter plot showing the relative volume occupied by GFP^+ cells in a selected region of the remote region and the injury site at 24 hpci. Values of endocardial volume at the injury site are also represented in Figure 1L (black line = mean ± s.d, t-test, $***P<0.005$). (E) Volume rendering of injured ventricles of *ET33mi-60A; myl7mRFP* hearts, with endocardium labelled green and myocardium magenta, at indicated time points. Volume rendering movies are available in the expanded view section. (F) Scatter plot showing the evolution of injury-site volume after cryoinjury in *ET33-mi60a; myl7:mRFP* transgenic hearts, quantified with IMARIS. (G-I) IHC against GFP and Pcna on sections of *ET33-mi60a* transgenic hearts (no ci, 3 dpci, 5dpci), showing almost any Pcna-expressing endocardial cell in the non-injured heart but high abundance of proliferating cells within the injury site (is) at 3 and 5 dpci (white arrowheads). The boxed area is magnified in the right hand panel. The dotted lines demarcate the injured tissue. Scale bars: 50 μm in A; 200 μm in B, E; 100 μm in C, G, H, I; 5 μm in magnified views in A, 100 μm in B, 20 μm in C,G, I.

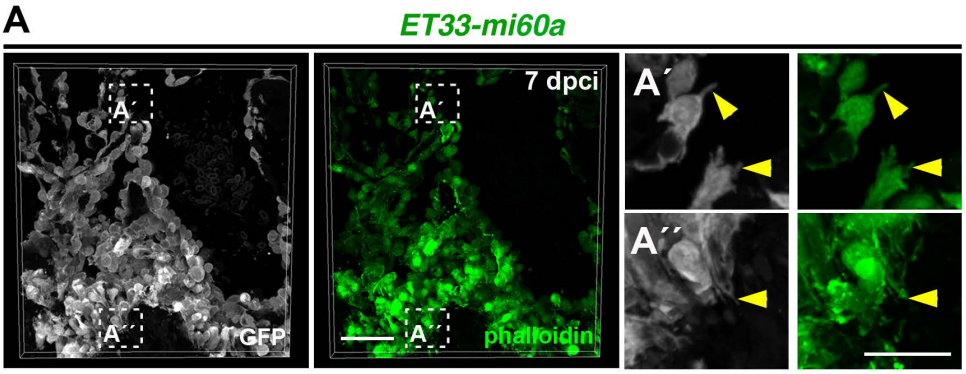

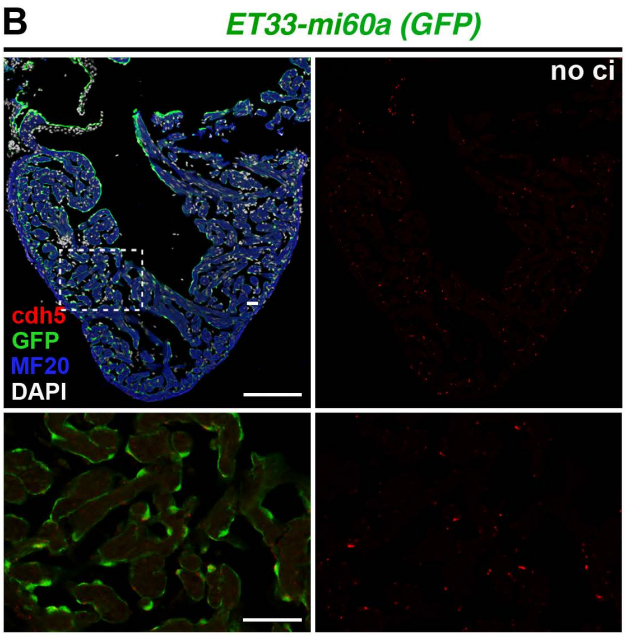

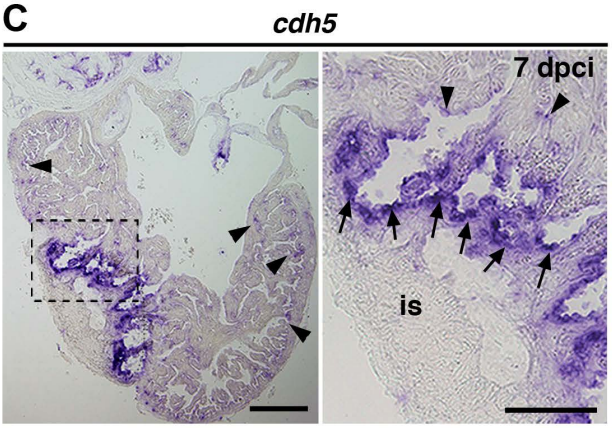

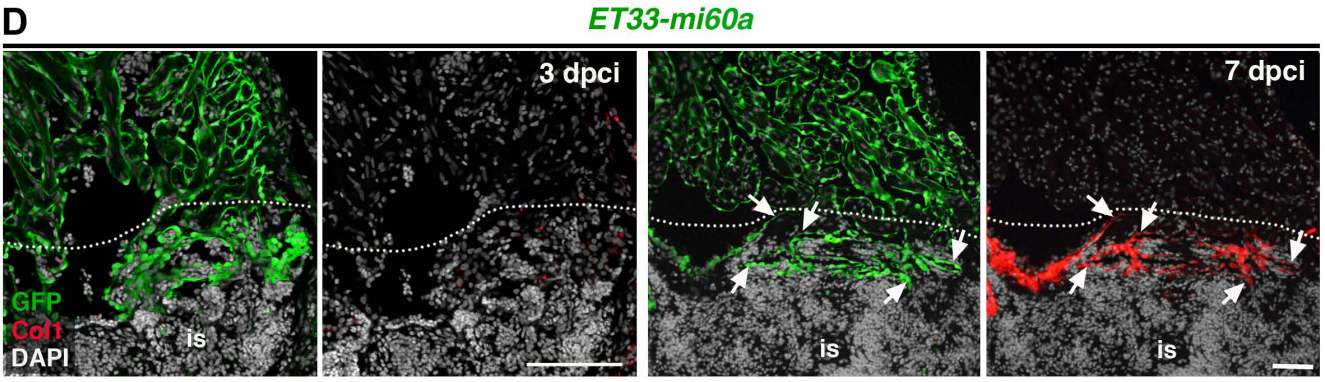

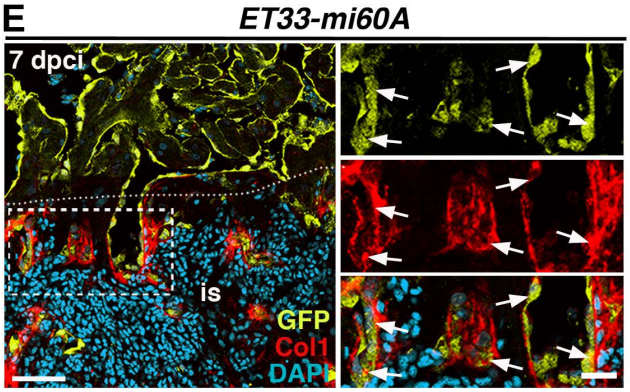

Fig. S2 The injury endocardium exhibits filopodia-like protrusions and high levels of cdh5

(A) Vibratome section of *ET33-mi60A* heart, immune-stained for GFP and with phalloidin (7 dpci). Filopodia-like protrusions of wound endocardial cells show phalloidin staining (A´, A´´, arrowheads) (B) *cdh5* FISH combined with IF showing low levels of *cdh5* levels (red) in GFP^+ endocardial cells all over the ventricle. (C) ISH against *cdh5* at 7 dpci, showing strong expression within the injury site (is, arrow) and weak expression in the remote region (arrowheads). Boxed areas are magnified below or on the right. (D, E) IHC against GFP and Col1 on sections of *ET33-mi60a* transgenic hearts, showing low Col1 signal at 3 dpci (B) and similar distribution of endocardial cells and col1 at the inner injury border (dotted line) at 7dpci (C, white arrowheads). Scale bars: 50 μm in A, E; 200 μm in B, C; 100 μm in D, 25 μm in magnified views in A, E, 50 μm in B, C.

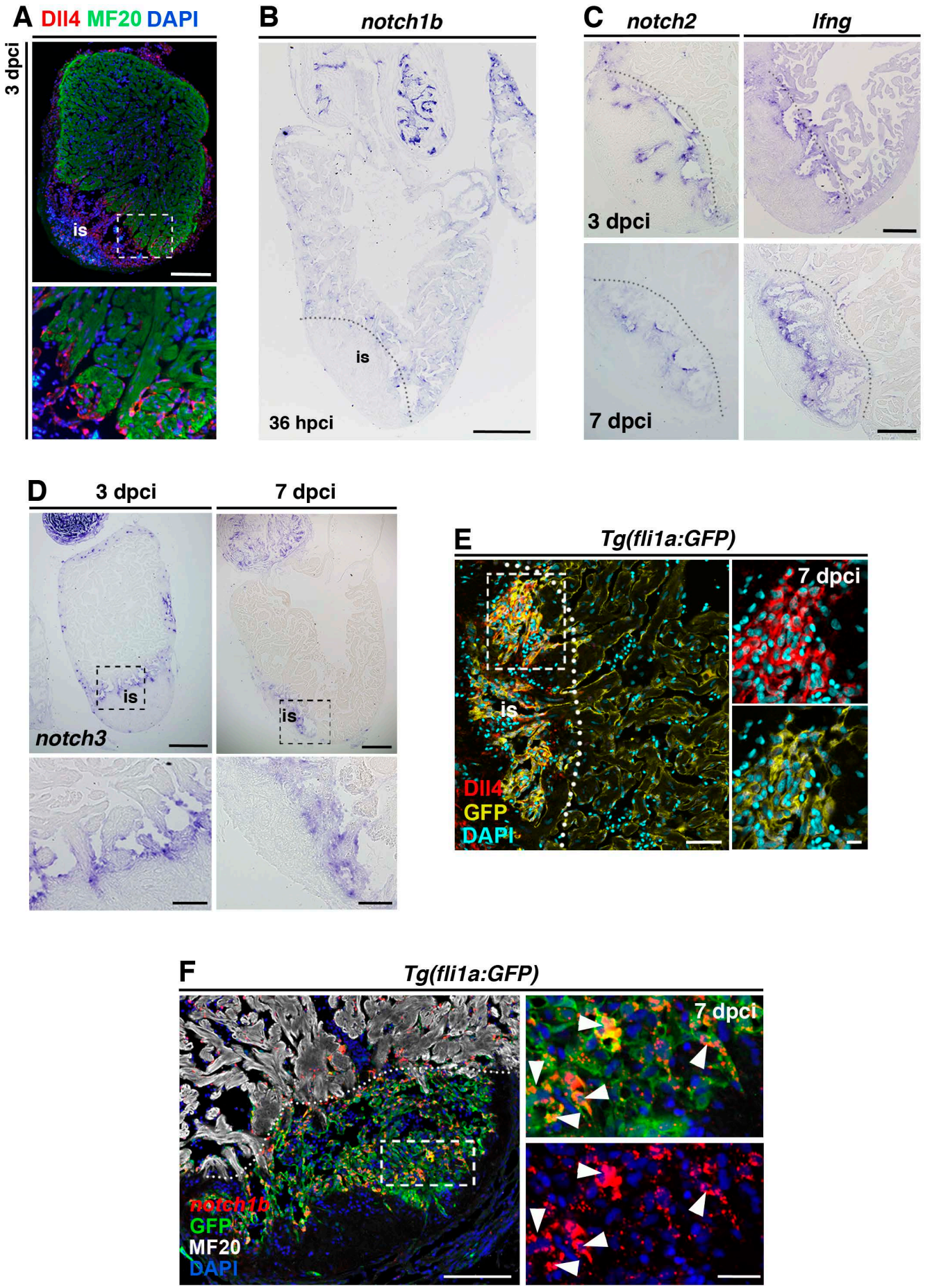

Fig. S3: Genes encoding Notch signalling elements are expressed in endocardial cells upon cryoinjury

(A) IHC of Dll4 and MF20, showing expression within the injury site (is) and surrounding adjacent cardiomyocytes. The boxed area is magnified in the panel below. (B) ISH for *notch1b*, showing low *notch1b* expression in the injury site and the remote region at 36 hpci. The dotted line demarcates the injury site (is). (C, D) ISH of *lfng*, *notch2* and *notch3* in regenerating hearts, showing expression adjacent to and within the injury site (is; 3 dpci, 7 dpci). Boxed areas are shown at higher magnification in the lower row. (E) IHC against Dll4 and GFP on sections of *Tg(fli1a:GFP)* transgenic hearts (7 dpci), showing endocardial expression of Dll4 (white arrowheads). The dotted line demarcates the injury site (is). (F) FISH against *notch1b* combined with IHC against GFP and MF20 on sections of *Tg(fli1a:GFP)* transgenic hearts (7 dpci) showing *notch1b* transcripts in endocardial cells (white arrowheads). The boxed area is magnified in the right-hand panels. The dotted line demarcates the injury site (is). (Scale bars: 200 μm in A, B; 100 μm in C, D, E, F; 50 μm in magnified views in A, D; 20 μm in E, F.

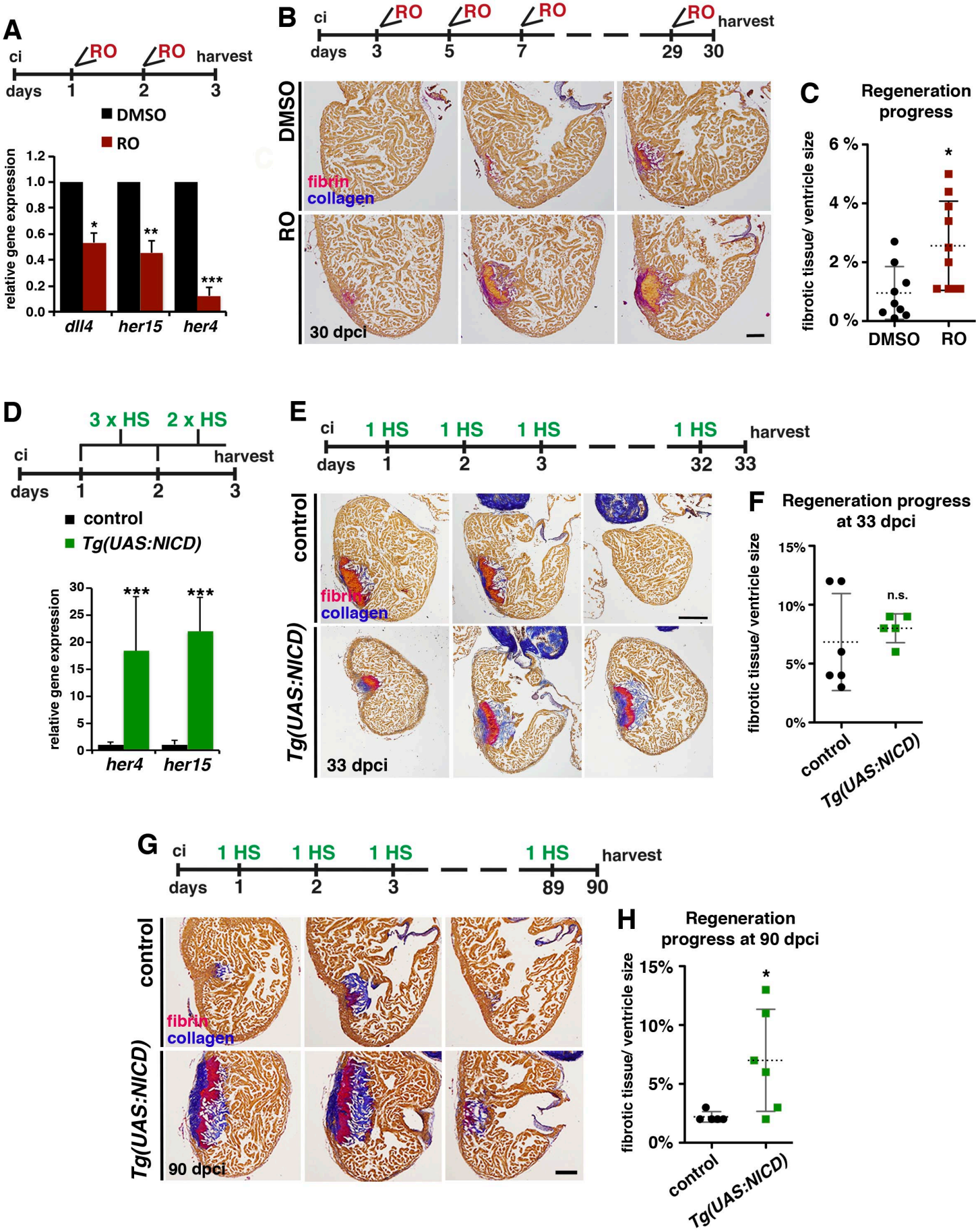

Figure S4_Münch et al.

Fig. S4: Notch signalling modulation impairs heart regeneration

(A) Relative gene expression (qPCR) of the Notch target genes *dll4*, *her15*, and *her4*, showing reduced expression after RO treatment (indicated on top). * $P<0.05$; ** $P<0.01$; *** $P<0.005$. (B) Representative AFOG-stained sections from three levels of the hearts of fish treated with DMSO or RO for 30 dpci (treatment regime is indicated on top). Cardiac muscle: brown; fibrin: pink/ orange; collagen: blue. (C) Scatter plot showing the amount of fibrotic tissue relative to ventricle size in hearts from fish treated with DMSO or RO (discontinuous line = mean ± s.d, t-test * $P<0.05$) (D) qPCR showing higher expression of *her4* and *her15* in injured hearts of transgenic *Tg(UAS:NICD)* fish compared than in the control at 3 dpci. (heat shock regime is indicated on top (mean ± s.d, t-test, *** $P< 0.005$). (E) AFOG–stained sections taken at 3 anatomical levels of WT and *Tg(UAS:NICD)* hearts at 33 dpci, showing similar regenerative capacity (heat shock regime is indicated on top). (F) Quantification of the progress of regeneration at 33 dpci (discontinuous line = mean± s.d, t-test, not significant). (G) AFOG-stained sections taken at 3 anatomical levels of WT and *Tg(UAS:NICD)* hearts at 90 dpci, showing failed regeneration (heat shock regime is indicated on top). (H) Quantification of the progress of regeneration at 90 dpci (discontinuous line = mean, t-test * $P<0.05$). Scale bars: 100 μm.

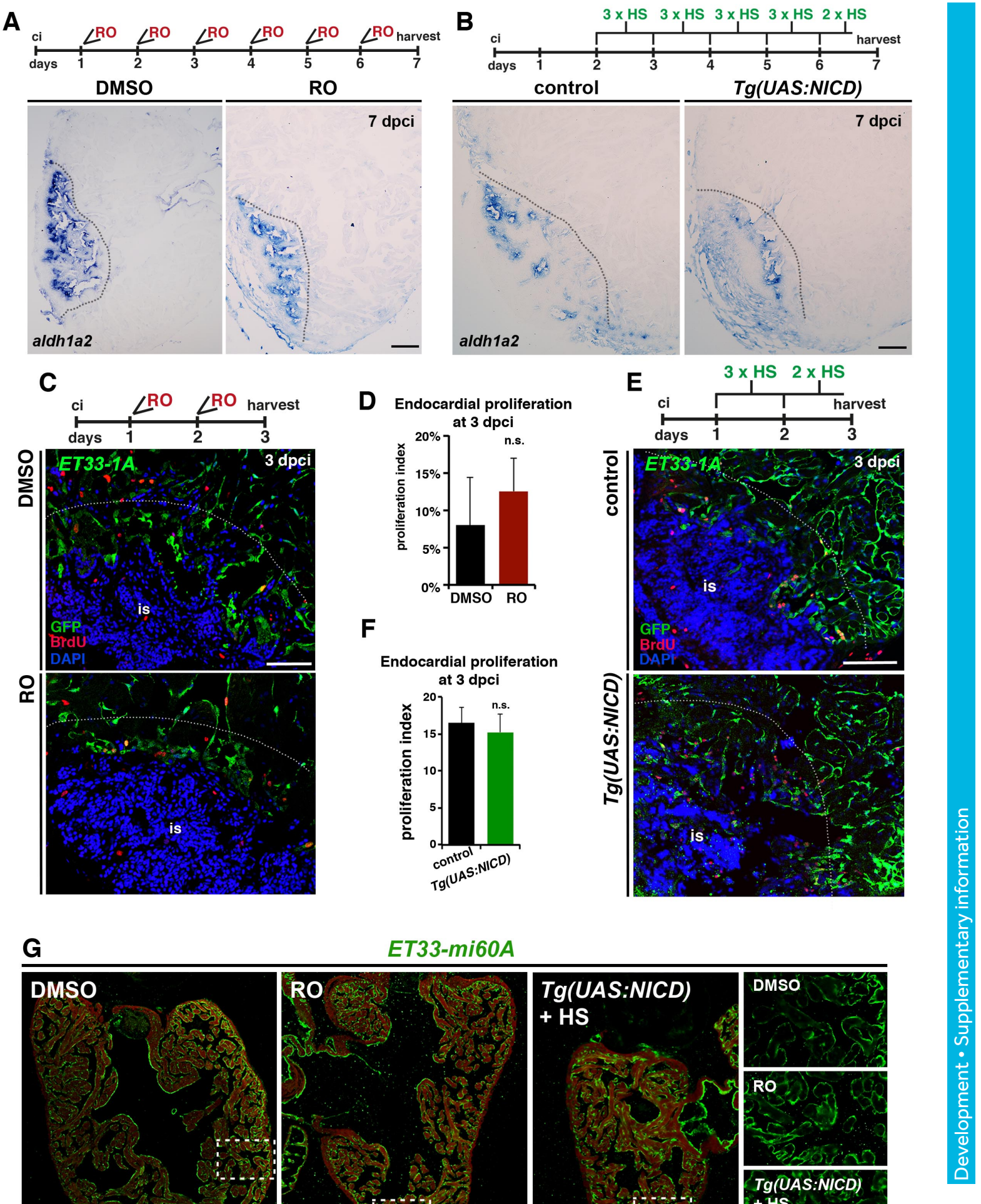

Fig. S5: Notch signalling modulation does not affect *aldh1a2* expression or proliferation

(A,B) ISH for *aldh1a2* on sections of hearts treated with DMSO or RO or from heat-shocked *Tg(UAS:NICD)* and control fish, showing no differences of expression. RO-treatment and heat shock regimes are indicated on top. (C) IHC against BrdU and GFP on heart sections of *ET33-1a* transgenic fish (3 dpci), showing BrdU incorporation by GFP^+ endocardial cells adjacent to the injury site (is). (D) Quantification of $BrdU^+$/ GFP^+ cell ratio in hearts of fish treated with DMSO or RO, indicating no difference in endocardial cell proliferation (mean± s.d, t-test, not significant). (E) IHC against BrdU and GFP on heart sections of *ET33-1a* transgenic fish alone or crossed with *Tg(UAS:NICD)* at 3 dpci, showing BrdU incorporation by GFP^+ endocardial cells adjacent to the injury site (is). (F) $BrdU^+$/ GFP^+ cell ratio in hearts of *ET33-1a* and *Tg(UAS:NICD); ET33-1a* transgenic fish, indicating no difference in endocardial cell proliferation (mean± s.d, t-test, not significant). (G) IHC for GFP and mf20 on sections of hearts treated with DMSO or RO or from heat-shocked *Tg(UAS:NICD)*, showing no differences of expression. Boxed areas are magnified on the right. Hearts were treated for 3 days with RO, DMSO or heat shocks. Scale bars: (A) 100 μm in all panels.

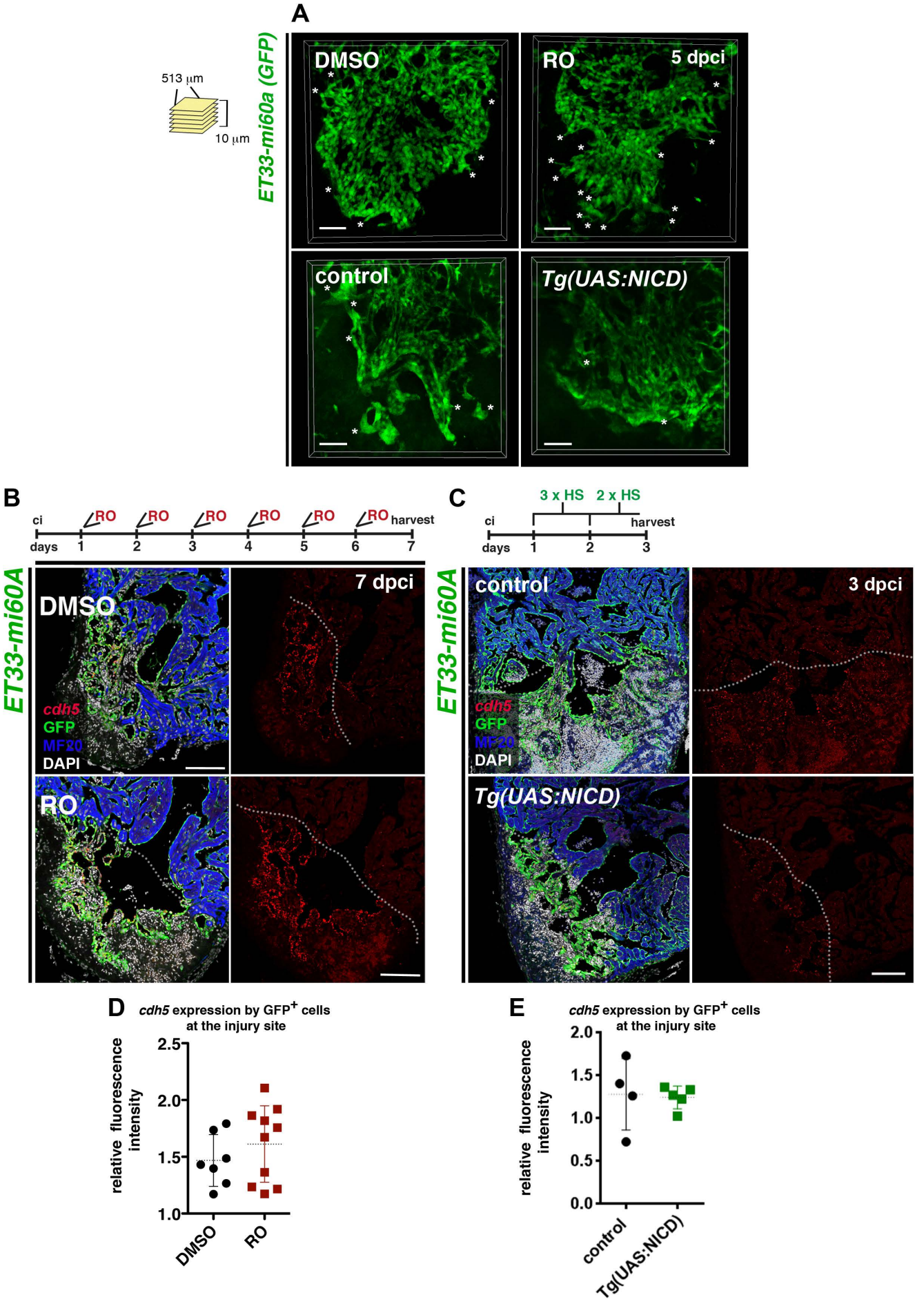

Fig. S6 Notch signalling modulation does not interfere with endocardial *cdh5*-expression

(A) Volume rendering of part of the injured region (513 µm x 513 µm x 10 µm) from *ET33mi-60A; myl7mRFP* hearts after treatment with RO or DMSO and from *ET33mi-60A; myl7mRFP, Tg(UAS:NICD)* and control hearts. Comparable 3D-images were used for quantification of filopodia- like protrusions. The graph of quantified filopodia is shown in Figure 3I. (B, C) FISH against *cdh5* combined with IHC against GFP and mf20 on sections of *ET33-mi60a* transgenic hearts after treatment with DMOS or RO (7dpci) and of *ET33mi-60A;Tg(UAS:NICD)* and control hearts (3dpci). The treatment regime is indicated on top. GFP^{+} endocardial/endothelial cells at the injury site present similar levels of *cdh5* expression in injured hearts after treatment with RO or DMSO and in *ET33mi-60A;Tg(UAS:NICD)* or control hearts. (D, E) Scatter plot showing relative red fluorescence intensity, comparing values of the endocardium of the remote region to the injury endocardium (see Figure 2D), in injured hearts (dotted line = mean± s.d, t-test, not significant). Scale bars: 50 µm in A, 100 µm in B, C.

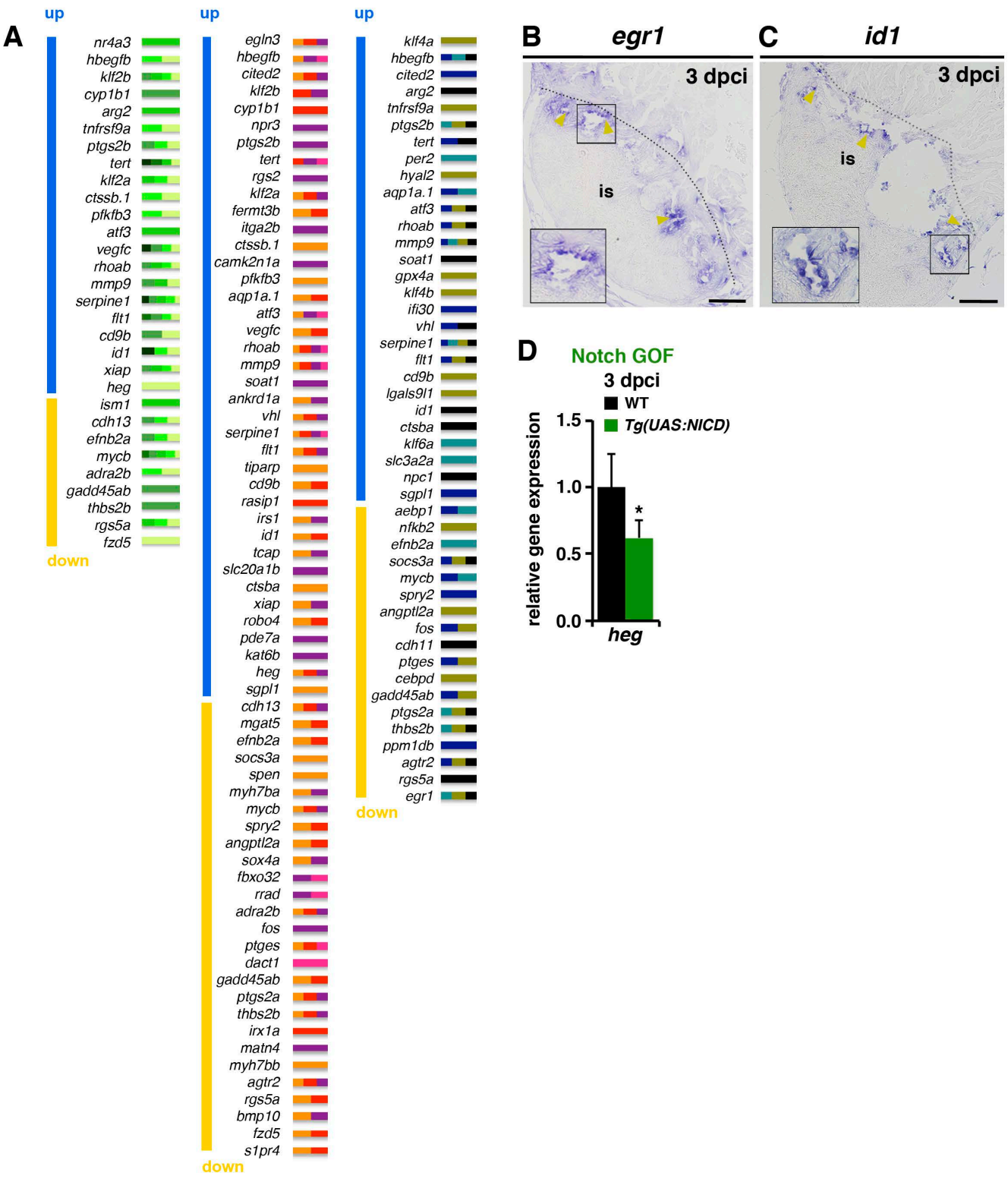

Fig. S7: Notch signalling affects endocardial/endothelial gene expression

(A) Genes assigned to the three categories in (Figure 4I). Genes are ordered according to their level of differential expression (up-regulated upon RO-treatment, blue; down-regulated, yellow). The colour of small bars indicates the assigned Ingenuity categories (presented in the chart in Figure 4C). (B, C) ISH,

showing *egr1*- and *id1*- expression at the inner injury border (yellow arrowheads). The boxed area is magnified in inserts. (D) qPCR analysis showing lower *heg* mRNA levels in *Tg(UAS:NICD)* transgenic injured ventricles than in control. (mean± s.d., t-test, **P*<0.05). Dotted lines delineate the injury site (is). Scale bars: 100 μm.

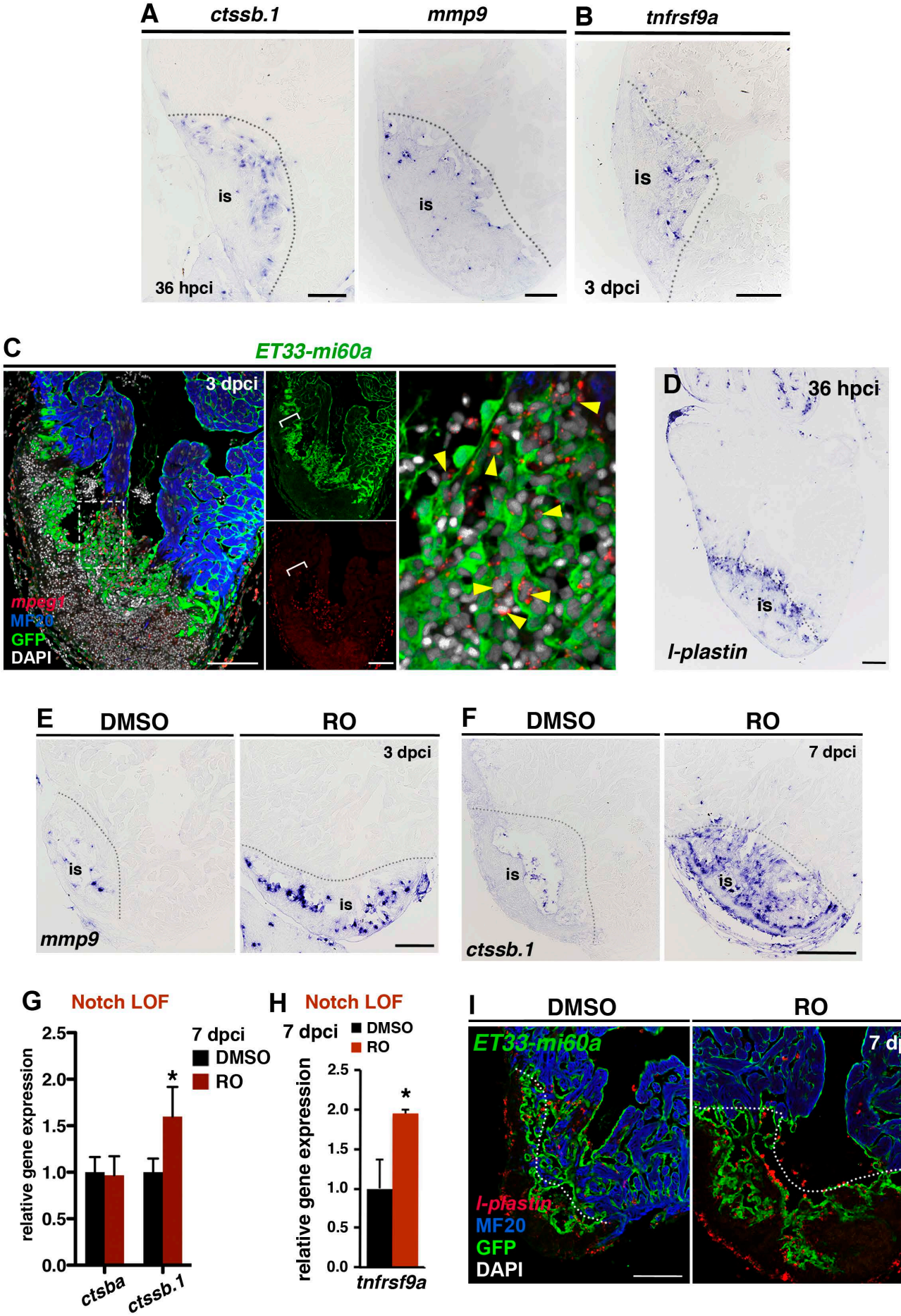

Fig. S8: Notch inhibition affects ECM remodelling gene expression and inflammatory processes

(A) ISH for *ctssb.1* and *mmp9*, revealing high expression at the inner injury border at 36 hpci. (B) ISH against *tnfrsf9a* on sections from an injured ventricle at 3 dpci, showing gene expression in cells with endocardial morphology within the injury site. (C) *mpeg1*- FISH combined with IHC, showing *mpeg*$^{+}$ cells (yellow arrowheads) in contact with GFP^{+} cells. *mpeg1*$^{+}$ cell accumulations at the injury site (is) locally coincides with high endocardial cell abundance (brackets). (D) ISH on consecutive sections for *l-plastin* showing high *l-plastin* expression in the injury site at 36 hpci. (E) ISH against *mmp9* (3 dpci), showing high numbers of positive cells within the injury site (is) of RO-treated hearts. (F) ISH against *ctssb.1* (7 dpci), showing high numbers of positive cells within the injury site (is) of RO-treated hearts. (G) qPCR analysis showing increased *ctssb.1* mRNA levels in injured ventricles at 7 dpci after RO-treatment. (mean± s.d., t-test, **P*<0.05. (H) qPCR analysis of *tnfrsf9a* expression in ventricles at 7 dpci after treatment with RO or DMSO mean± s.d., t-test, **P*<0.05). (I) FISH against *l-plastin* combined with IHC against GFP and MF20 on sections of *ET33-mi60a* transgenic hearts (7 dpci) after RO- or DMSO-treatment. RO-treatment results in an increased abundance of l-plastin^{+} macrophages associated to the endocardium. Dotted lines delineate the injury site (is). Scale bars: 100 µm.

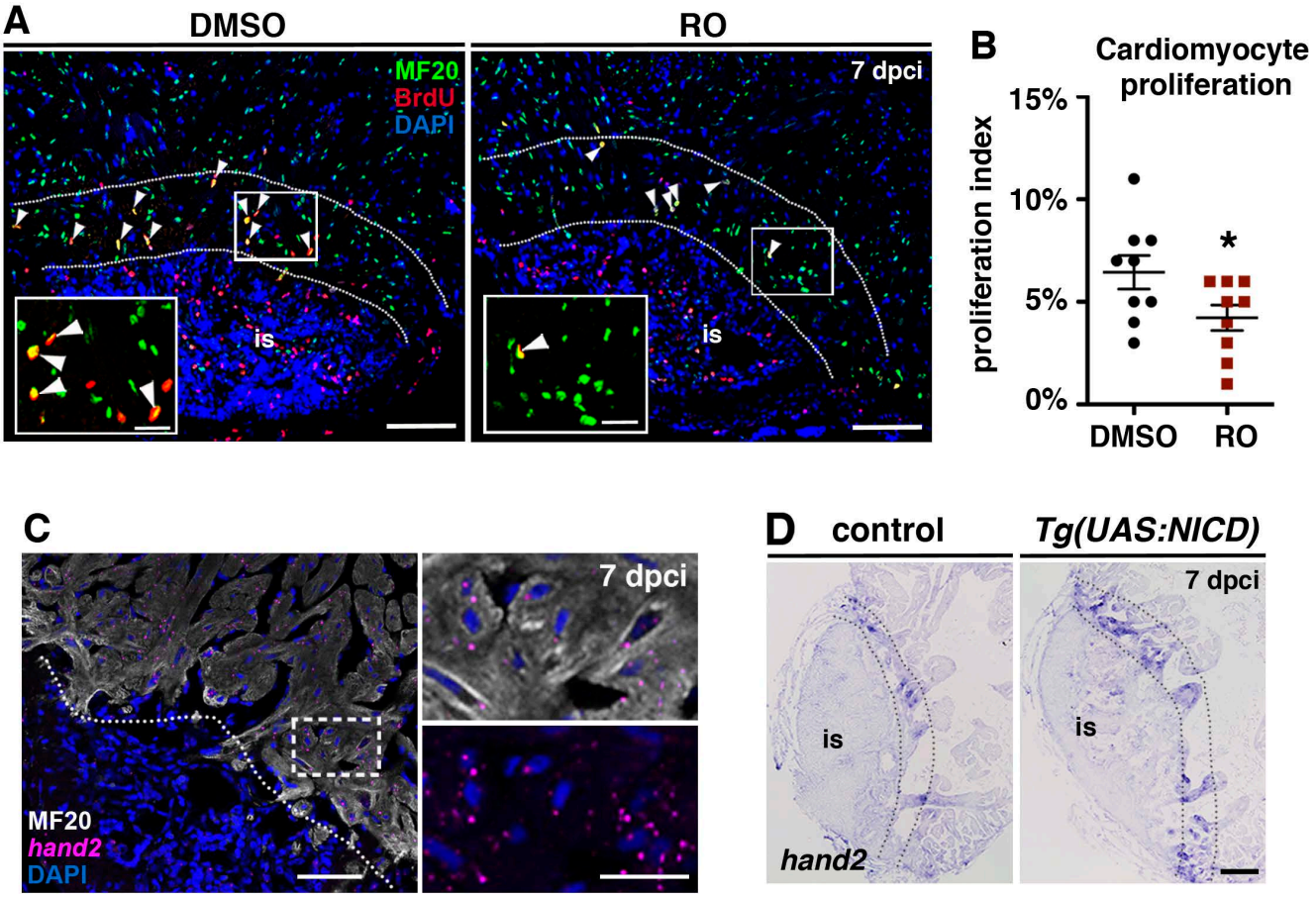

Fig. S9: Notch inhibition decreases cardiomyocyte proliferation

(A) IHC against BrdU and Mef2 on heart sections (7 dpci), showing lower BrdU incorporation in $Mef2^+$ cells (white arrowheads) adjacent to the injury (between the dashed lines) after treatment with RO than after treatment with DMSO. (B) Scatter plot showing quantification of $BrdU^+$ $Mef2^+$ cells in DMSO- and RO-treated hearts (discontinuous line = mean ± s.d., t-test, $*P<0.05$). (C) FISH against *hand2* combined with IHC for mf20 showing, *hand2*-expression in cardiomyocytes. (D) ISH against *hand2* at 7 dpci, showing higher numbers of injury-adjacent cardiomyocytes expressing these genes (between the dotted lines) in *Tg(UAS:NICD)* hearts than in control hearts. Dotted lines delineate the injury site (is). Scale bars: 100 µm; 25 µm in amplified views.

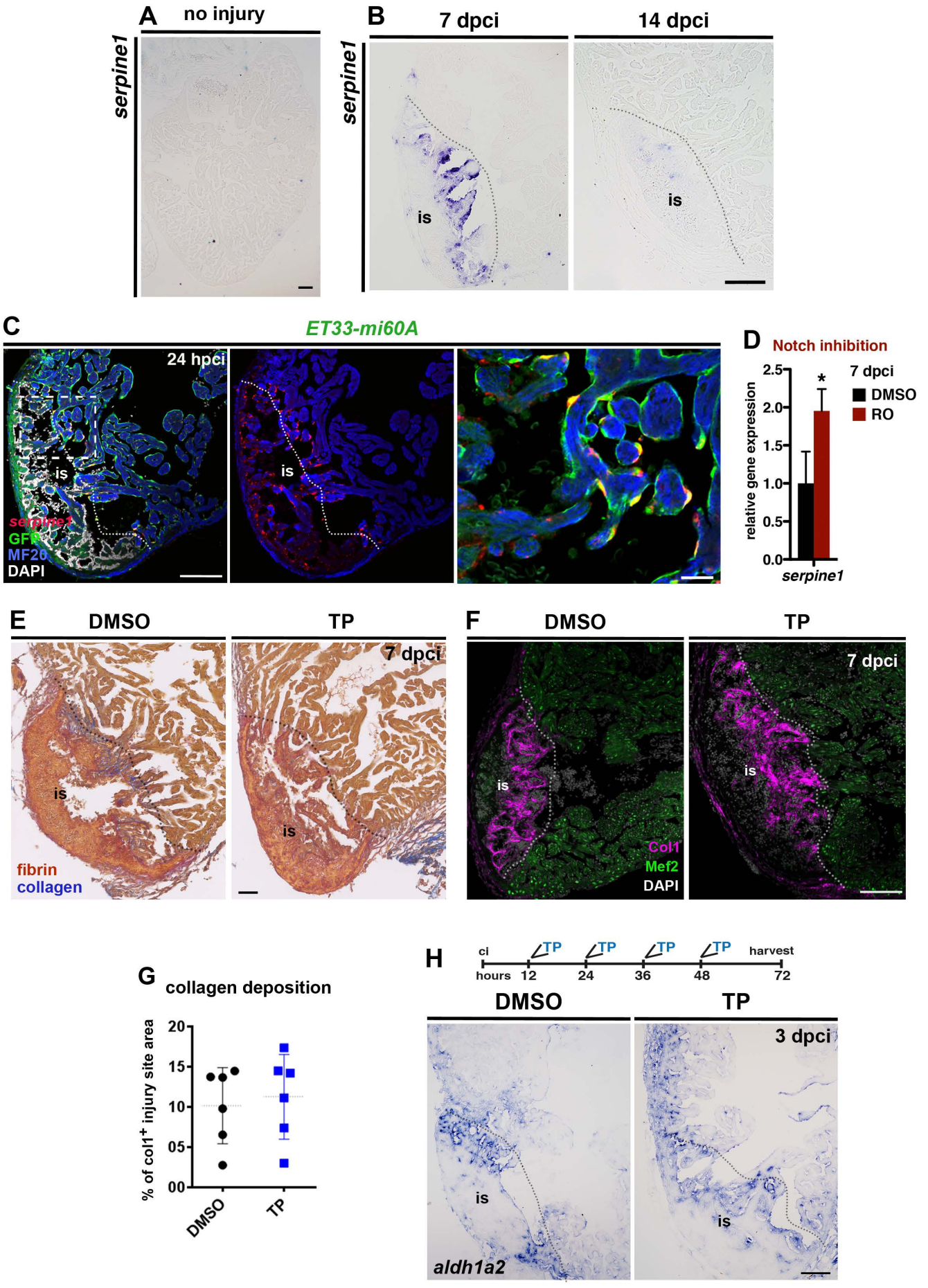

Fig. S10 Serpine1 is upregulated in the injury endocardium and its inhibition does not interfere with blood clot or collagen deposition.

(A, B) ISH against *serpine1*, showing no expression in the uninjured heart, moderate levels at 7 dpci but almost no expression at 14 dpci. (C) FISH against *serpine1* combined with IHC against GFP and MF20 on sections of *ET33-mi60a* transgenic hearts at 24 hpci. Serpine1 is strongly expressed in GFP^+ endocardial cells adjacent and within the injury site but not in remote regions at 24 hpci. The boxed area is magnified on the right hand panel. (D) qPCR analysis showing higher *serpine1* mRNA levels in injured ventricles at 7 dpci in RO-treated fish than in DMSO-treated fish (mean± s.d., t-test, $*P<0.05$). (E) AFOG stained TP- or DMSO treated hearts indicating similar fibrin deposition at the injury site (is) in both groups at 7dpci. (F) IHC for collagen 1 (Col1) and Mef2 showing similar amount of collagen at the injury site upon TP or DMSO-treatment. (G) Scatter plot showing the area covered by collagen relative to the injury site area in hearts treated with TP or DMSO. (dotted line = mean± s.d, t-test, not significant). (H) ISH in hearts treated with TP or DMSO (regime is indicated on top) showing similar expression of *aldh1a2* in the injury endocardium. Dotted lines delineate the injury site (is). Scale bar: 100 μm; 20 μm in the amplified view in C.

Supplemental Tables

Table S1: Sample numbers Figure 1-7 (Excell file attached)

Click here to Download Table S1

Table S2: Sample numbers Figure S1- S10 (Excell file attached)

Click here to Download Table S2

Table S3: Newman-Keuls Multiple Comparison Test for relative GFP^+ cell volume at indicated time points (Figure 1L)

Sample comparison	Significant? P < 0.05?	Summary
24 hpci vs 3 mpci	Yes	***
24 hpci vs 1 mpci	Yes	***
24 hpci vs 7 dpci	Yes	***
24 hpci vs 9 dpci	Yes	***
24 hpci vs 5 dpci	Yes	***
24 hpci vs 3 dpci	No	**ns**
24 hpci vs 36 hpci	No	**ns**
36 hpci vs 3 mpci	Yes	***
36 hpci vs 1 mpci	Yes	***
36 hpci vs 7 dpci	Yes	***
36 hpci vs 9 dpci	Yes	***
36 hpci vs 5 dpci	Yes	**
36 hpci vs 3 dpci	No	**ns**
3 dpci vs 3 mpci	Yes	***
3 dpci vs 1 mpci	Yes	***
3 dpci vs 7 dpci	Yes	***
3 dpci vs 9 dpci	Yes	***
3 dpci vs 5 dpci	Yes	**
5 dpci vs 3 mpci	Yes	***
5 dpci vs 1 mpci	Yes	*
5 dpci vs 7 dpci	No	**ns**
5 dpci vs 9 dpci	No	**ns**
9 dpci vs 3 mpci	Yes	**
9 dpci vs 1 mpci	No	**ns**
9 dpci vs 7 dpci	No	**ns**
7 dpci vs 3 mpci	Yes	*
7 dpci vs 1 mpci	No	**ns**
1 mpci vs 3 mpci	Yes	*

Table S4: Newman-Keuls Multiple Comparison Test for relative GFP^+ cell proliferation at indicated time points (Figure 1N)

Sample comparison	Significant? *P*<0.05?	Summary
24 hpci vs 3 dpci	Yes	***
24 hpci vs 5 dpci	Yes	*
24 hpci vs 36 hpci	No	ns
24 hpci vs 7 dpci	No	ns
7 dpci vs 3 dpci	Yes	***
7 dpci vs 5 dpci	Yes	*
7 dpci vs 36 hpci	No	ns
36 hpci vs 3 dpci	Yes	***
36 hpci vs 5 dpci	Yes	*
5 dpci vs 3 dpci	Yes	***

Table S5: Newman-Keuls Multiple Comparison Test for relative *serpine1*$^+$/ GFP^+ cells at indicated time points (Figure 7D)

Sample comparison	Significant? P < 0.05?	Summary
7 dpci vs 24 hpci	Yes	***
7 dpci vs 36 hpci	Yes	***
7 dpci vs 3 dpci	Yes	*
3 dpci vs 24 hpci	Yes	***
3 dpci vs 36 hpci	Yes	***
36 hpci vs 24 hpci	No	ns

Table S6: RNA-seq data of RO- *vs.* DMSO-treated wild type regenerating hearts 3 dpci (Excell file attached)

Click here to Download Table S6

Table S7: Primers used for RNA probe generation

Gene	forward	reverse
serpine1	GTT TGCTGAAGCCGTCCAGT	TCCACGCCATCCTTAGACAC
ctssb.1	GATGAAAATGCCCTCAAGCAG	AAGATAAGACGCACTTGGAT
myc-b	TTT ACC ACG GCT ACG GCA CT	CGG ATT CGC TGT CAC TAC TG
tnfrsf9a	TACGGAAAACTCAGAGTCCA	TTTGAGTATTCTCTCCCCAA
mpeg1	AACTCAGAGATCATCATGTCG	TGCCCTGATAACTACTGCTT
heg	CATTCAGGTACTGCGAACGACA	TACAACTGCGGCCATCCTC
egr1	CTTGCTGGAGATACGCTTTC	GGCTGCTGACCCGCTTGTGT
id1	CACTATCGACAACTCAACAAGCC	ACGTCACGCTTGTCATGTCCA
mylk3	GAGCCCACACATGTCCAGA	CTGTTGTTTCCATCCCCAT
tnfrsf9a	TACGGAAAACTCAGAGTCCA	TTTGAGTATTCTCTCCCCAA

Table S8: qPCR primers (*Danio rerio*)

Gene	forward	reverse
cathepsin B, a	GCACGACTGCCATACACAAG	GGCTGAGATCACACACAGGA
ctssb.1	CCAGATTCACTGGATTGGAGA	CCAACAAGAACCACAAGCAC
elf1a	CAGCTGATCGTTGGAGTCAA	TGTATGCGCTGACTTCCTTG
heg	TTGGAGGTTTCAACTGCAATAA	GCAATGACCACAATCAACAGA
her15	TCGCTCTGCTCAGAAACA	ACCACTGGCTTTCGAAT
her4.1	CAGAGAAACTCTACTGACAAACAAGC	GCTGCTGTTGATTCGCTCT
her6	GGCTTCGGAACACAGAAAGT	TGACCCAAGCTTTCGTTGA
hyal2	TTTGTCTACAGCCGCCCTAC	CAATGGTGGACACCAGATCA
klf2a	CCGTCTATTTCCACATTTTCG	TCCAGTTCATCCTTCCACCT
klf2b	CGTGGACATGGCTTTACCTT	TTGTGCTCCTCAATCTTCCA
mmp9	TGCTCTCCCAGCTGTCATC	CCACTGTAAACCCAGAACTGTCT
myc-b	TGTTTCCCTTTCCACTGAC	CTTCATCATCTTCGTCATCG
mylk3	AAGTTGAGTCGACACTGCTGAT	ACAATGCGATGGTCGAATG
rpsm	GATGGCGGACACTCAGAAC	CCAATCCAACGTTTCTGTGA
serpine1	GTCTATTCCAAGGTTCTCCAT	CTGAAAATGTCTCCAAGACC
sgpl1	CCATTATTATGAAGAATCCGAAAGA	CATCGATCGGTCAGGAATG
tcap	GGGACGATCAATGTCTCAGG	CGTCCATAAAGTCTTTGACTCATATTT
tnfrsf9a	AACTGGACTCCTTCAGGAAAAA	TCTTTTCACCAAGCGGTTTC

Table S9: qPCR primers (*Sus scrofa*)

Gene	forward	reverse
SERPINE1	TACACTGAGTTTTCCACCC	AATGAACATGCTCAGAGTG
GAPDH	ACACTCACTCTTCTACCTTTG	CAAATTCATTGTCGTACCAG

Supplementary References

Chen, J., Huang, C., Truong, L., La Du, J., Tilton, S. C., Waters, K. M., Lin, K., Tanguay, R. L. and Dong, Q. (2012). Early life stage trimethyltin exposure induces ADP-ribosylation factor expression and perturbs the vascular system in zebrafish. *Toxicology* **302**, 129-139.

Chen, J. N. and Fishman, M. C. (1996). Zebrafish tinman homolog demarcates the heart field and initiates myocardial differentiation. *Development* **122**, 3809-3816.

Gonzalez-Rosa, J. M., Martin, V., Peralta, M., Torres, M. and Mercader, N. (2011). Extensive scar formation and regression during heart regeneration after cryoinjury in zebrafish. *Development* **138**, 1663-1674.

Kanzler, B., Kuschert, S. J., Liu, Y. H. and Mallo, M. (1998). Hoxa-2 restricts the chondrogenic domain and inhibits bone formation during development of the branchial area. *Development* **125**, 2587-2597.

Kikuchi, K., Holdway, J. E., Major, R. J., Blum, N., Dahn, R. D., Begemann, G. and Poss, K. D. (2011). Retinoic acid production by endocardium and epicardium is an injury response essential for zebrafish heart regeneration. *Developmental cell* **20**, 397-404.

Larson, J. D., Wadman, S. A., Chen, E., Kerley, L., Clark, K. J., Eide, M., Lippert, S., Nasevicius, A., Ekker, S. C., Hackett, P. B. et al. (2004). Expression of VE-cadherin in zebrafish embryos: a new tool to evaluate vascular development. *Developmental dynamics : an official publication of the American Association of Anatomists* **231**, 204-213.

Lawson, N. D. and Weinstein, B. M. (2002). In vivo imaging of embryonic vascular development using transgenic zebrafish. *Developmental biology* **248**, 307-318.

Luxan, G., Casanova, J. C., Martinez-Poveda, B., Prados, B., D'Amato, G., MacGrogan, D., Gonzalez-Rajal, A., Dobarro, D., Torroja, C., Martinez, F. et al. (2013). Mutations in the NOTCH pathway regulator MIB1 cause left ventricular noncompaction cardiomyopathy. *Nature medicine* **19**, 193-201.

Munch, J., Gonzalez-Rajal, A. and de la Pompa, J. L. (2013). Notch regulates blastema proliferation and prevents differentiation during adult zebrafish fin regeneration. *Development* **140**, 1402-1411.

Poon, K. L., Liebling, M., Kondrychyn, I., Garcia-Lecea, M. and Korzh, V. (2010). Zebrafish cardiac enhancer trap lines: new tools for in vivo studies of cardiovascular development and disease. *Developmental dynamics : an official publication of the American Association of Anatomists* **239**, 914-926.

Prince, V. E., Holley, S. A., Bally-Cuif, L., Prabhakaran, B., Oates, A. C., Ho, R. K. and Vogt, T. F. (2001). Zebrafish lunatic fringe demarcates segmental boundaries. *Mechanisms of development* **105**, 175-180.

Rohr, S., Otten, C. and Abdelilah-Seyfried, S. (2008). Asymmetric involution of the myocardial field drives heart tube formation in zebrafish. *Circulation research* **102**, e12-19.

Scheer, N., Groth, A., Hans, S. and Campos-Ortega, J. A. (2001). An instructive function for Notch in promoting gliogenesis in the zebrafish retina. *Development* **128**, 1099-1107.

Susaki, E. A., Tainaka, K., Perrin, D., Kishino, F., Tawara, T., Watanabe, T. M., Yokoyama, C., Onoe, H., Eguchi, M., Yamaguchi, S. et al. (2014). Whole-brain imaging with single-cell resolution using chemical cocktails and computational analysis. *Cell* **157**, 726-739.

Vermot, J., Forouhar, A. S., Liebling, M., Wu, D., Plummer, D., Gharib, M. and Fraser, S. E. (2009). Reversing blood flows act through klf2a to ensure normal valvulogenesis in the developing heart. *PLoS biology* **7**, e1000246.

Westin, J. and Lardelli, M. (1997). Three novel Notch genes in zebrafish: implications for vertebrate Notch gene evolution and function. *Development genes and evolution* **207**, 51-63.

Wong, K. S., Rehn, K., Palencia-Desai, S., Kohli, V., Hunter, W., Uhl, J. D., Rost, M. S. and Sumanas, S. (2012). Hedgehog signaling is required for differentiation of endocardial progenitors in zebrafish. *Developmental biology* **361**, 377-391.

Yelon, D., Ticho, B., Halpern, M. E., Ruvinsky, I., Ho, R. K., Silver, L. M. and Stainier, D. Y. (2000). The bHLH transcription factor hand2 plays parallel roles in zebrafish heart and pectoral fin development. *Development* **127**, 2573-2582.

Yoshinari, N., Ishida, T., Kudo, A. and Kawakami, A. (2009). Gene expression and functional analysis of zebrafish larval fin fold regeneration. *Developmental biology* **325**, 71-81.

Zhang, R., Han, P., Yang, H., Ouyang, K., Lee, D., Lin, Y. F., Ocorr, K., Kang, G., Chen, J., Stainier, D. Y. et al. (2013). In vivo cardiac reprogramming contributes to zebrafish heart regeneration. *Nature* **498**, 497-501.

Supplementary Movies

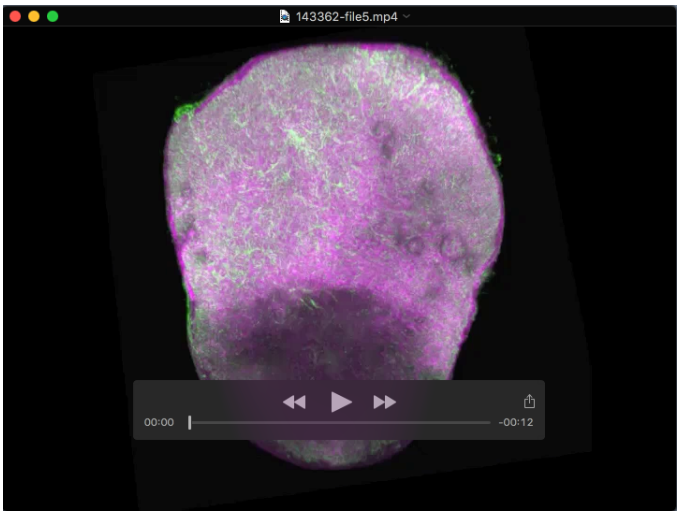

Movie 1: IMARIS volume rendering of a whole mount *ET33-mi60a* (green); *myl7:mRFP*(magenta) cryoinjured transgenic heart at 24 hpci.

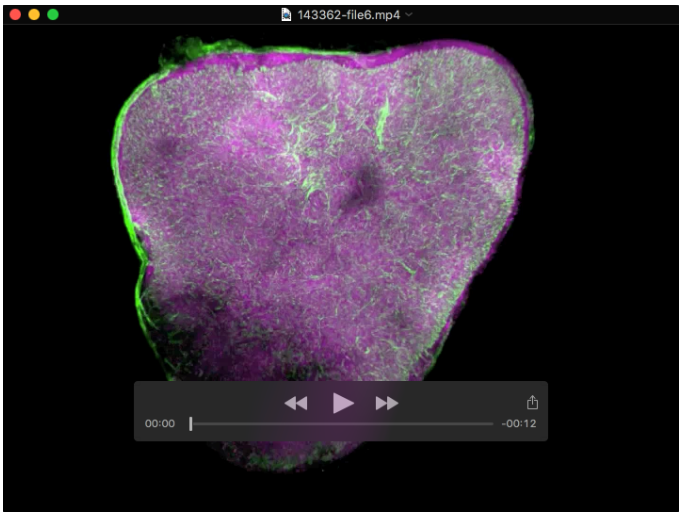

Movie 2: IMARIS volume rendering of a whole mount *ET33-mi60a* (green); *myl7:mRFP*(magenta) cryoinjured transgenic heart at 36 hpci.

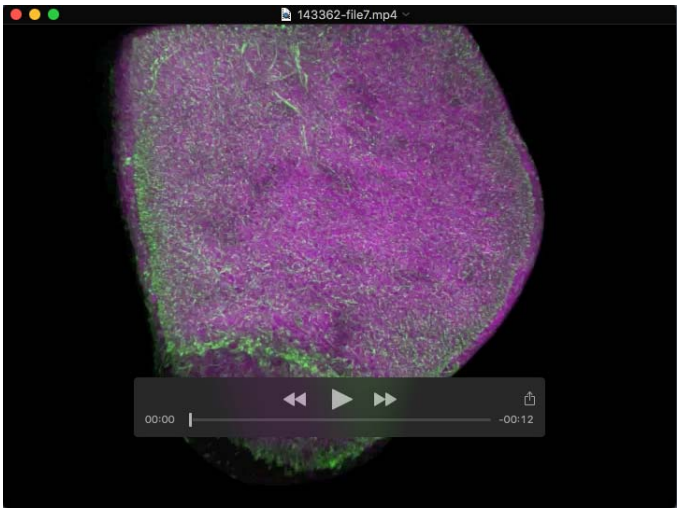

Movie 3: IMARIS volume rendering of a whole mount *ET33-mi60a* (green); *myl7:mRFP*(magenta) cryoinjured transgenic heart at 3 dpci.

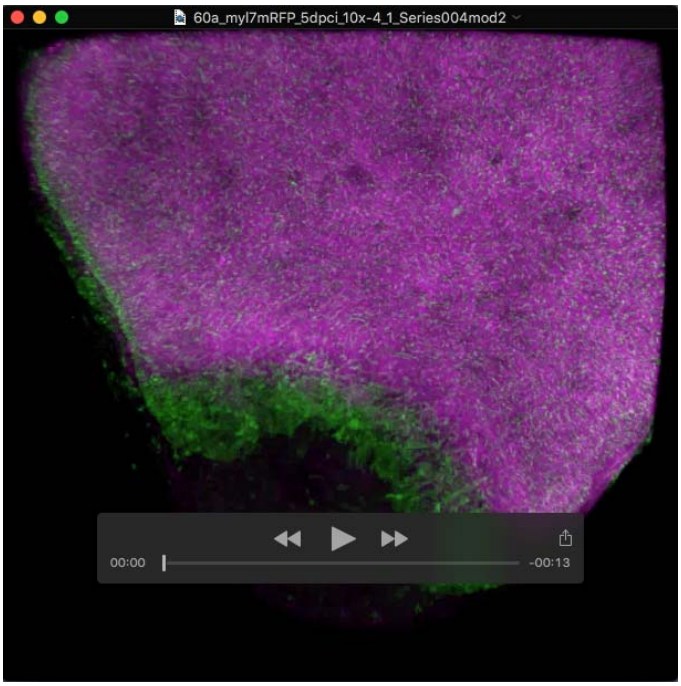

Movie 4: IMARIS volume rendering of a whole mount *ET33-mi60a* (green); *myl7:mRFP*(magenta) cryoinjured transgenic heart at 5 dpci.

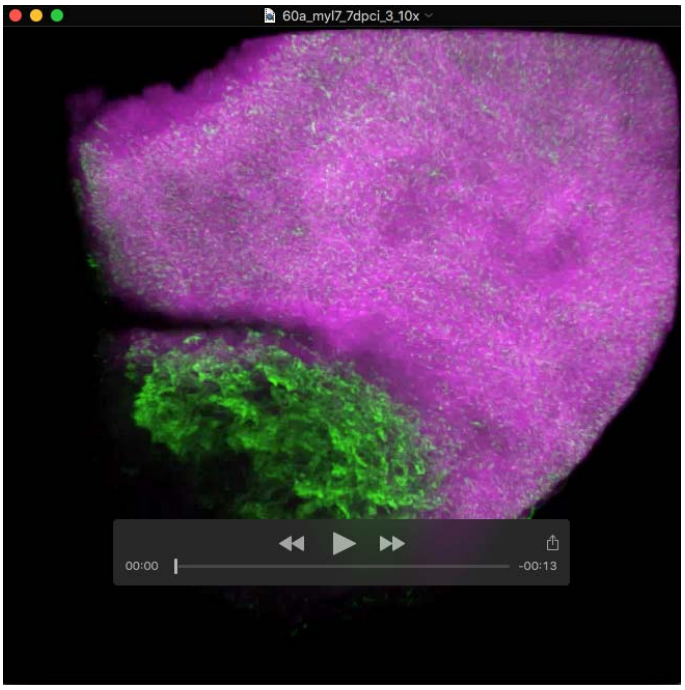

Movie 5: IMARIS volume rendering of a whole mount *ET33-mi60a* (green); *myl7:mRFP*(magenta) cryoinjured transgenic heart at 7 dpci.

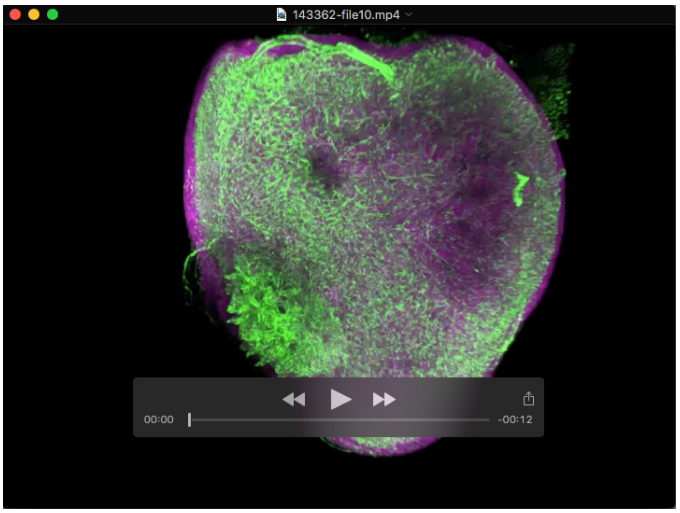

Movie 6: IMARIS volume rendering of a whole mount *ET33-mi60a* (green); *myl7:mRFP*(magenta) cryoinjured transgenic heart at 9 dpci.

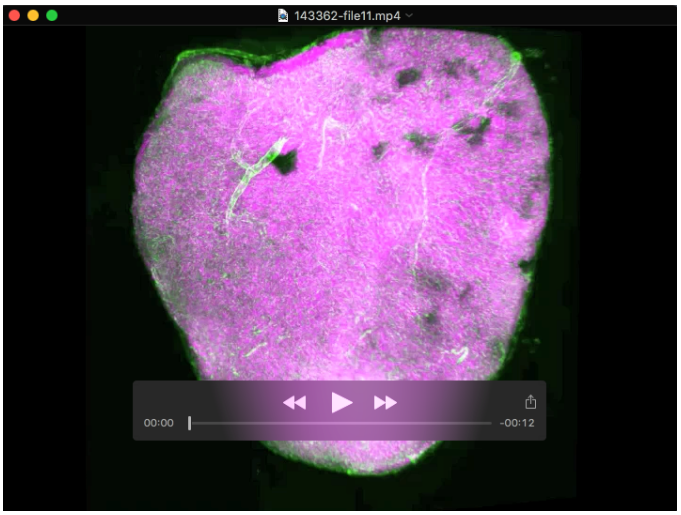

Movie 7: IMARIS volume rendering of a whole mount *ET33-mi60a* (green); *myl7:mRFP*(magenta) cryoinjured transgenic heart at 1 mpci.

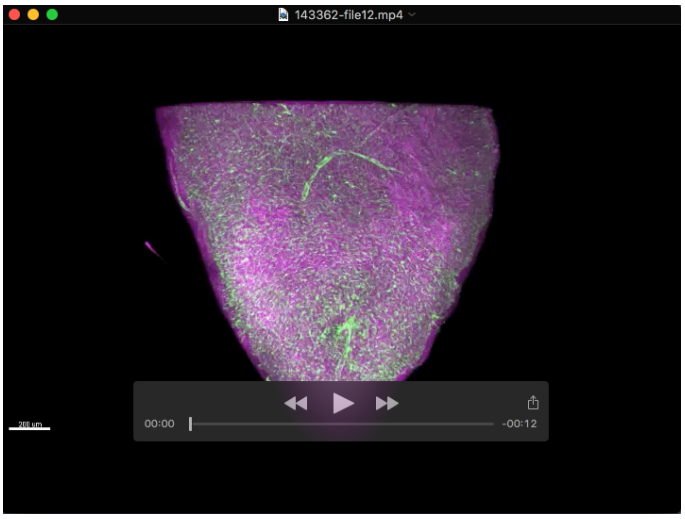

Movie 8: IMARIS volume rendering of a whole mount *ET33-mi60a* (green); *myl7:mRFP*(magenta) cryoinjured transgenic heart at 3 mpci.

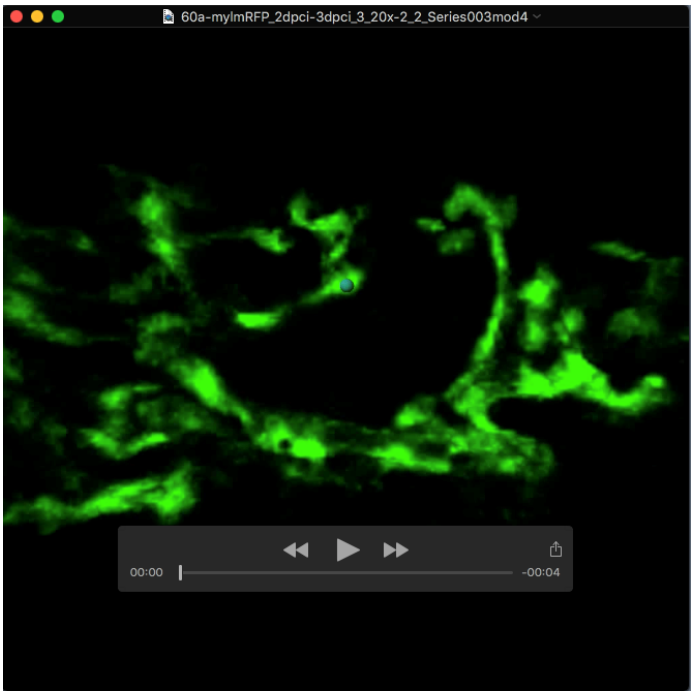

Movie 9: Confocal 3D time-lapse movie of endocardial cells of a selected area within the injury site in *ET33-mi60a* (green); *myl7:mRFP* (magenta) cryoinjured transgenic heart at around 56 hpci. Individual cells migrate and change their collocation. Still images can be found in Figures 2H.

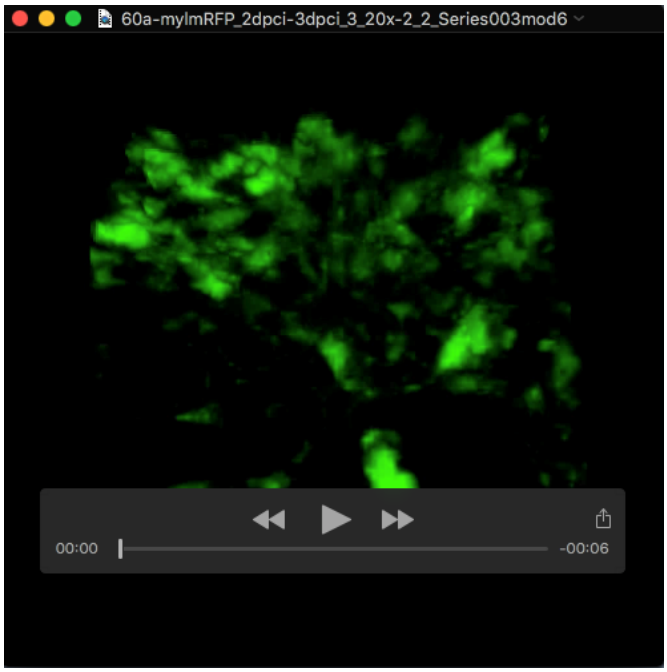

Movie 10: Confocal 3D time-lapse movie of endocardial cells of a selected area within the injury site in *ET33-mi60a* (green); *myl7:mRFP* (not shown) cryoinjured transgenic heart at around 56 hpci. Individual cells migrate and send out filopodia-like protrusions. Still images can be found in Figures 2I.